Ligand Substitution and Addition Reactions of Transient Radical Cations Generated by the Electrochemical Oxidation of $(\eta\text{-}C_5H_5)(CO)_2FeMe$ in Acetone

Hong-Ye Liu, M. Neal Golovin, Deborah A. Fertal, Audrey A. Tracey, Klaas Eriks, Warren P. Giering,* and Alfred Prock*

Department of Chemistry, Metcalf Center for Science and Engineering, Boston University, Boston, Massachusetts 02215

Received October 12, 1988

The chemistry resulting from the oxidation of $(\eta\text{-Cp})(CO)_2FeMe$ (1) in acetone at low temperatures was probed via cyclic voltammetry and computer simulation. The results are consistent with the following picture: At −86 °C, the electrochemical oxidation of $(\eta\text{-Cp})(CO)_2FeMe$ in acetone (0.1 M lithium perchlorate) affords a kinetically determined and nearly equimolar mixture of the iron(III) complexes $(\eta\text{-Cp})(CO)(AC)FeCOMe^+$ (2^+, AC = acetone) and $(\eta\text{-Cp})(CO)(ClO_4)FeCOMe$ (3) which decomposes rapidly to 2^+. The iron(II) perchlorate complex 3^-, which is short-lived, is not observed electrochemically and decomposes, in part, to the neutral acetone complex 2. At higher temperatures, 2 decomposes with activation parameters of $\Delta S^\ddagger = -2.8 \pm 7.8$ eu and $\Delta H^\ddagger = 13.1 \pm 1.8$ kcal/mol. In the iron(II) state, reaction of the acetone complex 2 with thioanisole to form the sulfide complex $(\eta\text{-Cp})(MeSPh)(CO)FeCOMe$ (4) proceeds through a dissociative pathway whereas the transformation of the perchlorate complex 3^- to 4, which is at least 100 times faster, proceeds via a different reaction pathway. In the iron(III) state the substitution of acetone in 2^+ by thioanisole proceeds via an entering ligand dependent pathway; the perchlorate complex 3 is not directly transformed to 4^+.

Introduction

Trogler[1] presented evidence in support of a suggestion by Grubbs[2] that the alkyl to acyl migratory insertion reactions of $(\eta\text{-Cp})(CO)(L)FeMe^+$ involve transient 19-electron heptacoordinate (hypervalent) complexes $(\eta\text{-Cp})(CO)(L)(L')FeMe^+$ (where L′ is the incoming ligand). This interpretation is in accord with the results of kinetic[3] and theoretical[4] studies of coordinatively saturated 18-electron alkylmetal carbonyls which suggest that in these systems the rearrangement is nucleophilically assisted. Recently, we showed that the oxidation of $(\eta\text{-Cp})(CO)_2FeMe$ (1) at −78 °C in mixtures of acetonitrile and methanol generated $(\eta\text{-Cp})(CO)(AN)FeCOMe^+$ and $(\eta\text{-Cp})(CO)(MeOH)FeCOMe^+$ in proportions that reflect the solvent composition.[5] In contrast to the aforementioned suggestion, we concluded that the rearrangement of $(\eta\text{-Cp})(CO)_2FeMe^+$ to $(\eta\text{-Cp})(CO)(sol)FeCOMe^+$ either involves an early transition state with little metal solvent bonding or proceeds via a transition state that does not involve the solvent. Clearly, the dynamic role of a coordinating solvent is not well-understood. Accordingly, we have extended our studies[6] to the oxidation of $(\eta\text{-Cp})(CO)_2FeMe$ (1) in the poorer coordinating solvent acetone in order to shed further light on the nature of the highly reactive transients involved in this reaction.

Results

The cyclic voltammogram of $(\eta\text{-Cp})Fe(CO)_2Me$ (1) in acetone (0.1 M $LiClO_4$) at −41 °C shows an initial oxidation wave (E_p = 1.2 V) followed by a second multiple electron oxidation with no sharp peak; no significant return waves were observed on scan reversal to −0.5 V. Similar results are obtained when only the first anodic wave is traversed. Predicated on our previous observations[5] that the initial oxidations of 1 are often complicated by secondary chemical and electrochemical processes, we ramped only the foot of the initial anodic wave without traversing the peak. Under these condition we observed a new couple near 0.0 V. In order to maximize the concentration of the species responsible for the waves at 0.0 V, we performed a series of step/hold and scan (SHS) experiments. In a typical SHS experiment, the potential was stepped to 0.92 V (on the foot of the first anodic wave of $(\eta\text{-Cp})Fe(CO)_2Me$) and held there for 5.0 s; the potential was then swept in the negative direction. The resulting curve (Figure 1) exhibits a quasi-reversible couple (E° = −0.016 V) which we attribute to the acetone complexes $(\eta\text{-Cp})(CO)(AC)FeCOMe^{+,0}$ (AC = acetone; $2^{+,0}$). Although 2^+ can be detected up to 0 °C via cyclic voltammetry, its neutral partner 2 is less stable and is observable only at much lower temperatures. We investigated the effect of variation of the initial hold potential on the features of the resulting cyclic voltammograms in the SHS experiments at −41 °C. From 0.85 to 1.10 V there is little change in the overall voltammograms except for the expected increase in the current of the cathodic waves for 2^+. With hold potentials above 1.10 V we observed the appearance of several additional cathodic waves and an attenuation of the anodic return wave for the $2^+/2$ couple. The concentration of 1 was varied over a factor of 4 from 5.0 to 20 mM over a temperature range from −87 to −41 °C. The relative shapes of the cyclic voltammograms obtained via SHS experiments are independent of the concentration of 1, thereby indicating that the kinetics of the system are first order in iron complexes.

We do not have direct evidence for the structure of 2 but the oxidation of $(\eta\text{-Cp})Fe(CO)_2Me$ (1) in other coordinating solvents is known to afford solvent incorporated acetyl complexes.[1,5,6] A distinctive feature[7] of these acetyl

(1) Therien, M. J.; Trogler, W. C. *J. Am. Chem. Soc.* **1987**, *109*, 5127.
(2) Doxsee, K. M.; Grubbs, R. H.; Anson, F. C. *J. Am. Chem. Soc.* **1984**, *106*, 7819.
(3) (a) Webb, S. L.; Giandomenico, C. M.; Halpern, J. *J. Am. Chem. Soc.* **1986**, *108*, 345. (b) Wax, M. J.; Bergman, R. G. *J. Am. Chem. Soc.* **1981**, *103*, 7028.
(4) Axe, F. U.; Marynick, D. S. *Organometallics* **1987**, *6*, 572-580.
(5) Golovin, M. N.; Meirowitz, R. E.; Rahman, Md. M.; Prock, A.; Giering, W. P. *Organometallics* **1987**, *6*, 2285-89.
(6) (a) Javaheri, S.; Giering, W. P. *Organometallics* **1984**, *3*, 1927. (b) Magnuson, R. H.; Meirowitz, R. E.; Giering, W. P. *Organometallics* **1983**, *2*, 460. (c) Magnuson, R. E.; Meirowitz, R. E.; Zulu, S. J.; Giering, W. P. *J. Am. Chem. Soc.* **1982**, *104*, 5790. (d) Magnuson, R. H.; Zulu, S. J.; T'sai, W.-M.; Giering, W. P. *J. Am. Chem. Soc.* **1980**, *102*, 6887.
(7) Gowda, N. M. N.; Naikar, S. B.; Reddy, G. K. N. *Adv. Inorg. Chem. Radiochem.* **1984**, *28*, 255-99.

0276-7333/89/2308-1454$01.50/0

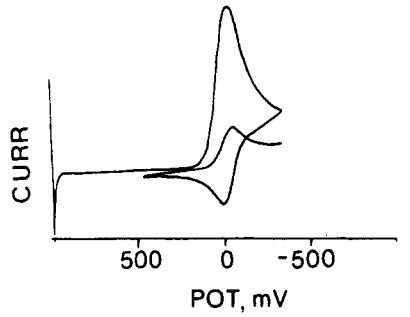

Figure 1. Cyclic voltammogram of (η-Cp)$(CO)_2$FeMe in acetone (0.1 M $LiClO_4$) at −41 °C observed after the initial potential was held at 0.92 V for 5 s and then swept in the negative direction to −0.3 V before being reversed and swept to ~0.3 V. Scan rate is 100 mV s^{-1}.

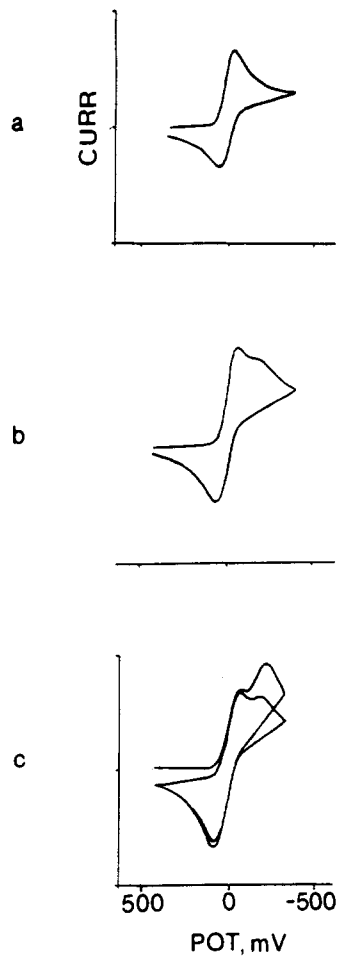

Figure 2. Cyclic voltammograms of (η-Cp)$(CO)_2$FeMe at −87 °C with a scan rate of 500 mV s^{-1}: (a) CV's obtained on sample dissolved in acetone containing 0.1 M $LiPF_6$, (b) with added $LiClO_4$, and (c) in a 1:1 mixture of acetone/methylene chloride containing 0.1 M $LiClO_4$.

complexes is their acetyl carbonyl stretching frequencies that occur around 1700–1730 cm^{-1}. Unfortunately, we are not able to observe a similar band for the acetone complex because of the masking of this region by the intense carbonyl absorption of the solvent. The reduction potential, $E°$ (−0.016 V), for the acetone complex is, however, similar to the $E°$ (−0.07 V) observed for the methanol complex[5] (η-Cp)(CO)(MeOH)$FeCOMe^+$, lending further support to our structural assignment.

Below −75 °C the electrochemical behavior of the system is complicated by appearance of a new cathodic wave (lacking an anodic return wave) with a peak potential more

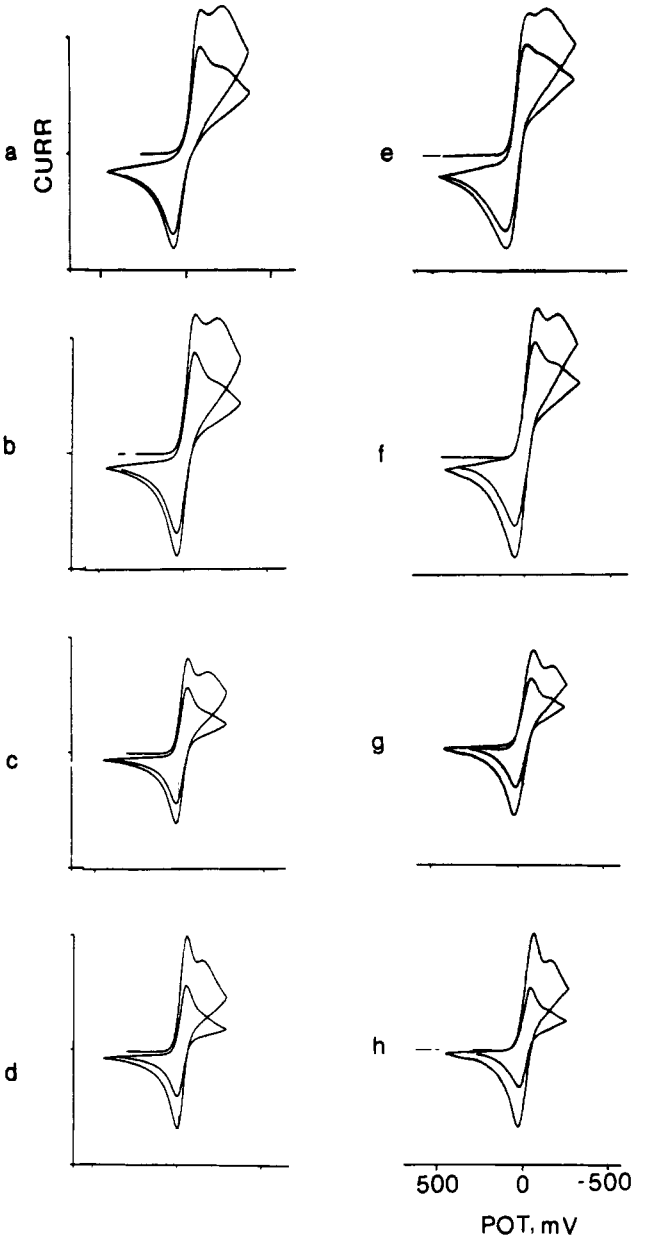

Figure 3. Simulated (a–d) and experimental (e–h) CV's of (η-Cp)$(CO)_2$FeMe in acetone containing 0.1 M $LiClO_4$ at −87 °C with scan rates of 500 (a and e), 200 (b and f), 100 (c and g), and 50 mV s^{-1} (d and h).

negative than that of 2^+. We identify the species responsible for this new wave as the perchlorate complex **3**, (η-Cp)(CO)(ClO_4)FeCOMe (vide infra). The relative currents of the cathodic waves for 2^+ and **3** are not dependent upon the initial concentration of **1**; however, they are dependent on scan rates, with the cathodic wave for **3** being attenuated at the lower rates. We identify **3** as a perchlorate complex based on the following observations. Most important, the cathodic wave for **3** is absent when lithium hexafluorophosphate is substituted for lithium perchlorate as the supporting electrolyte (Figure 2a) Second, the addition of lithium perchlorate to the solution containing the lithium hexafluorophosphate causes the reappearance of the second cathodic wave (Figure 2b). Thirdly, the current ratio of the perchlorate complex to the acetone complex, $i(\mathbf{3})/i(\mathbf{2}^+)$, is dramatically increased when the SHS experiment is performed on a solvent mixture containing a lower concentration of acetone (1:1 methylene chloride/acetone, 0.1 M lithium perchlorate, Figure 2c). Finally, computer simulation of these experiments shows

that **3** converts to 2^+ and 3^- converts to **2** (vide infra) thereby suggesting that 2^+ and **3** possess related structures.

The electrochemical results were analyzed by computer simulation for scan rates of 0.05–0.5 V s^{-1}. In performing the computer analysis of the electrochemical results, we considered first a sequential process in which 1^+ was transformed to **3** and then to 2^+. We were unable to fit the simulations to the experimental data. A variety of other mechanisms were tried, but good results were obtained only when we allowed 2^+ and **3** to be formed simultaneously followed by conversion of **3** to 2^+ and 3^- to **2** (eq 1–10 in Scheme I). The rate constants and ratios of rate constants obtained by simulation are presented in Table I. A set of experimental curves and the analogous computer simulations are shown in Figure 3. The code for the simulation is provided in the supplementary materials. The experiments began by stepping the potential

Scheme I

$$(\eta\text{-Cp})(CO)_2FeMe \underset{}{\overset{E^\circ(1)}{\rightleftharpoons}} \underset{1}{1^+} \quad (1)$$

$$1^+ \xrightarrow{k_2} \underset{3}{Cp(CO)(ClO_4)FeCOMe} \quad (2)$$

$$1^+ \xrightarrow{k_3} \underset{2^+}{Cp(CO)(AC)FeCOMe^+} \quad (3)$$

$$3 + AC \xrightarrow{k_4} 2^+ + ClO_4^- \quad (4)$$

$$3 \xrightarrow{k_5} \text{decomposition} \quad (5)$$

$$3 \underset{}{\overset{E^\circ(3)}{\rightleftharpoons}} \underset{3^-}{Cp(CO)(ClO_4)FeCOMe^-} \quad (6)$$

$$3^- + AC \xrightarrow{k_7} \underset{2}{Cp(CO)(AC)FeCOMe} + ClO_4^- \quad (7)$$

$$3^- \xrightarrow{k_8} \text{decomposition} \quad (8)$$

$$2^+ \underset{}{\overset{E^\circ(2)}{\rightleftharpoons}} 2 \quad (9)$$

$$2 \xrightarrow{k_{10}} \text{decomposition} \quad (10)$$

$$2^+ + PhSMe \xrightarrow{k_{11}} \underset{4^+}{(\eta\text{-Cp})(CO)(PhSMe)FeCOMe^+} + AC \quad (11)$$

$$3 + PhSMe \xrightarrow{k_{12}} 4^+ + ClO_4^- \quad (12)$$

$$2 + PhSMe \xrightarrow{k_{13}} \underset{4}{(\eta\text{-Cp})(CO)(PhSMe)FeCOMe} + AC \quad (13)$$

$$3^- + PhSMe \xrightarrow{k_{14}} 4 + ClO_4^- \quad (14)$$

$$4^+ \underset{}{\overset{E^\circ(4)}{\rightleftharpoons}} 4 \quad (15)$$

of the electrode to 0.92 V, holding for 5 s and then scanning at a selected rate to a potential of –0.3 V. The scan was reversed and swept positive to 0.4 V and then back to –0.3 V and finally back to 0.4 V. This procedure results in a pair of cyclic voltammograms as shown in Figure 3e–h. The important features of these cyclic voltammograms must be (and are) fully accommodated by the simulations (Figure 3a–d). First, 3^- is short-lived since we are unable to observe a return wave for the reduction of **3** even at 8 V s^{-1} at –86 °C. Second, the cathodic wave for **3** on the second scan is greatly attenuated consistent with decomposition of **3** in the bulk during the course of the experiment. Third, currents of the waves for the $2^+/2^0$ couple in the second scan are a large fraction of the corresponding currents of the first cyclic voltammogram. This is particularly noticeable in the experiment performed at –86 °C in mixed (1:1) methylene chloride/acetone (Figure 2c). Owing to the nonuniform concentration profiles of the electrochemically active species generated by the SHS experiment, diffusion of material from the electrode should have diminished the currents in the second scan. That this is not observed indicates that there is generation of the acetone complexes after the initial oxidation.

Table I. Experimental Temperatures and Corresponding Rate Constants and Ratios of Rate Constants[a] Obtained by Computer Simulation for the Reactions Shown in the Reaction Scheme in the Absence of PhSMe

T, °C	k_2/k_3[b]	k_4, s^{-1}	k_5, s^{-1}	k_7/k_8[b]	k_{10}, s^{-1}
–86	1.35	0.033	0	0.50	
–75	1.06	0.095	0.01	0.87	
–56	*c*			0.06	0.02
–81					0.12
					0.15
–41					0.30
					0.40
–31					1.5
					1.6
					1.8

[a] We believe that these rate constant are accurate to within 10%. See text. [b] k_2, k_3, and k_8 must be at least 5 s^{-1}. [c] **3** is not observed at this or higher temperatures at scan rates less than 500 mV s^{-1}.

At higher temperatures, –56 to –31 °C, where **3** is not observed, we monitored the decomposition of **2** and obtained the activation parameters and the 95% confidence limits from an analysis of the kinetic data: $\Delta H^\ddagger$ = 13.1 ± 1.8 kcal/mol and $\Delta S^\ddagger$ = –2.8 ± 7.8 eu.

The addition of thioanisole at –75 °C to the reaction mixture containing $(\eta\text{-Cp})(CO)_2FeMe$ (**1**) in acetone (0.1 M lithium perchlorate) results in the generation of a new set of waves (E° = 0.203 V) which we assign to the $(\eta\text{-Cp})(CO)(SPhMe)FeCOMe^{0,+}$ ($4/4^+$) couple (Figure 4). Calibration of the system with ferrocene shows that the concentrations (0.26×10^{-2} to 2.6×10^{-2} M) of thioanisole were at least 5 times greater than the amount of **1** oxidized during the step part of the SHS experiment; therefore, in the simulation part of the analysis we did not correct for depletion of sulfide because of chemical reaction. At low concentrations of sulfide only small amounts of 4^+ are formed prior to the reduction of 2^+ or **3**. The amount of 4^+ does increase linearly with concentration of PhSMe. Direct generation of 4^+ from 1^+ is excluded in the proposed scheme because its inclusion gives simulated results which disagree with experimental data. The direct formation of 4^+ from 1^+ is kinetically distinct from its formation from 2^+ and 3^0. In contrast to 2^+ and 3^0, 1^+ exists only during the step and hold part of the experiment and cannot contribute to the formation of 4^+ during the sweep part of the experiment. Thus experiments done at different sweep rates serve to distinguish between these two cases.

For a given concentration of sulfide, **4** is formed in much larger concentrations after the reduction of 2^+ and **3**. The amount of **4** that is generated is also a function of the sulfide concentration.

In the absence of sulfide (–87 °C) the ratio k_3/k_2 (both rate constants are large) and the value of k_4 were obtained from the information contained in the first negative sweep for each of the four scan rates of the experiment. The remaining three sweeps for all four scan rates provided us with the values for k_7/k_8 and k_{10}. We found that a change

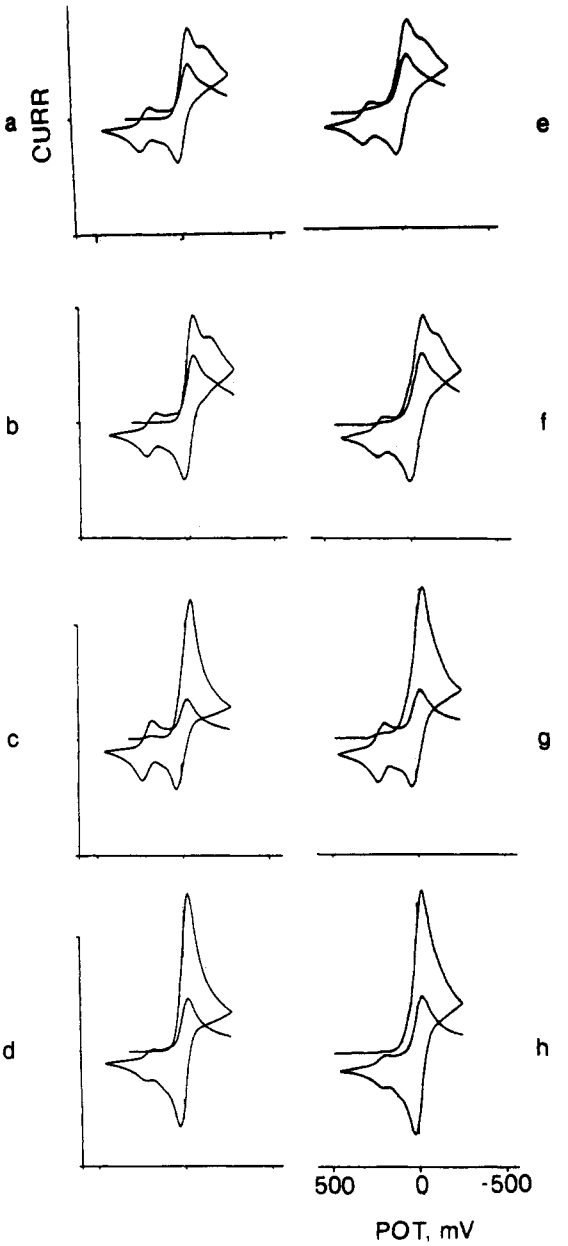

Figure 4. Simulated (a–d) and experimental (e–h) CV's of (η-Cp)$(CO)_2$FeMe in acetone containing 0.1 M $LiClO_4$ and various amounts of PhSMe at −75 °C: (a and e) 2.6×10^{-2} M PhSMe at 200 mV s^{-1}, (b and f) 1.3×10^{-2} M PhSMe at 200 mV s^{-1}, (c and g) 0.88×10^{-2} M PhSMe at 50 mV s^{-1}, and (d and h) 0.26×10^{-2} M PhSMe at 50 mV s^{-1}. Concentrations were determined at room temperature.

of 10% in the value of a rate constant or the ratio of rate constants produced a visually significant deviation of the computed cyclic voltammograms from the experimental ones.

For the experiments done at −75 °C at the slower scan rate (50 mV s^{-1}) the perchlorate complex **3** was absent, greatly simplifying the analysis. Results were insensitive to k_3, and it was simply made large (>4 s^{-1}). In the absence of sulfide, results depended only on k_{10}. In the presence of sulfide, k_{11} was obtained from the first negative sweep; k_{13} was obtained from the remaining sweeps at seven different concentrations. At the faster scan rate where **3** and $\mathbf{3}^-$ are present, only those rate constants (k_4) or their ratios (k_3/k_2) involving these species needed to be evaluated. Conversion of **3** to $\mathbf{4}^+$ is so rapid that we were able to set k_8 to zero and k_{14} to a large value (vide infra). The rate constants determined at −75 °C are $k_{11} = 0.004$ M^{-1} s^{-1} and $k_{12} = 0.0$. Results were insensitive to k_4 as long as it was made very large (>40 s^{-1}). The simulations are shown in Figure 4a–d, and the data for k_{13} are displayed in Figure 5.

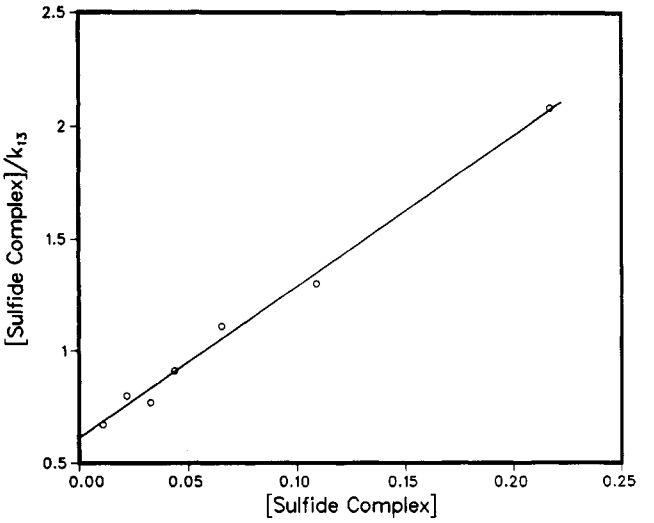

Figure 5. Plot of [PhSMe]/k_{13} versus [PhSMe] at −75 °C.

Interestingly, the neutral iron(III) perchlorate complex **3** does not appear to undergo significant conversion to the sulfide complex $\mathbf{4}^+$, whereas the anionic iron(II) perchlorate complex $\mathbf{3}^-$ is completely converted to **4** with apparently little conversion to the acetone complex **2**. Both acetone complexes $\mathbf{2}^+$ and **2** react with the sulfide to form $\mathbf{4}^+$ and **4** although the reaction in the iron(II) state at low concentrations of sulfide is about 100 times faster. For the iron(III) complex, a plot of k_{11}[sulfide] (the pseudo-first-order rate constant used in the simulations) versus [sulfide] is linear, whereas for the iron(II) complex a plot of k_{13} versus [sulfide] is nonlinear. The latter data plotted as [sulfide]/(k_{13}) versus [sulfide] is linear (the 95% confidence limits are given) with a slope of 6.74 ± 0.24 s and an intercept of 0.61 ± 0.09 Ms.

Discussion

Since perchlorate is undoubtedly a much poorer nucleophile than acetone, the observation of the perchlorate complex **3** was unexpected although not unprecedented.[7] The perchlorate complexes **3** and $\mathbf{3}^-$ are thermodynamically unstable with respect to the acetone complexes $\mathbf{2}^+$ and $\mathbf{2}^0$. It is obvious then that the initially formed mixture is kinetically determined. Previously, we proposed that the oxidation of (η-Cp)$(CO)_2$FeMe (**1**) generated a highly reactive electrophile which reacted indiscriminately with accessible nucleophiles. Furthermore, simulation analysis shows that both $\mathbf{2}^+$ and **3** are formed concurrently rather than sequentially. That perchlorate is able to compete with the solvent acetone (which is present in 100-fold excess) for the iron complex suggests that electrostatic interactions play an important role in this system. Thus, we propose that some $\mathbf{1}^+$ lives long enough to form an ion pair with perchlorate which subsequently converts to either the acetone ($\mathbf{2}^+$) or the perchlorate (**3**) complex. It is noteworthy that we do not observe **3** in methanol, which may reflect the greater solvating power of methanol as compared to acetone. At this stage we do not know if the rearrangement of $\mathbf{1}^+$ proceeds via the unsaturated acetyl complex or if it is solvent (or perchlorate) assisted. Whatever the case, it is clear that we are dealing with a very "hot" organometallic cation radical intermediate.

The conversions of the acetone complexes (**2** and $\mathbf{2}^+$) to the corresponding thioanisole complexes (**4** and $\mathbf{4}^+$) proceed

via different mechanisms at −75 °C. In the iron(III) state, 2^+ appears to undergo an entering ligand dependent substitution reaction with the sulfide. In contrast, the analysis of the kinetic data for the transformation of **2** into **4** is consistent with the dissociative process shown in eq 16 and 17. The rate equation for this process is given by eq 18. The relationship between k_{13} and k_{16}, k_{-16}, and k_{17} is given by eq 19. Thus, a plot of $[PhSMe]/k_{13}$ versus [PhSMe]

$$(\eta\text{-Cp})(CO)(AC)FeCOMe \underset{k_{-16}}{\overset{k_{16}}{\rightleftharpoons}} (\eta\text{-Cp})(CO)FeCOMe + AC \quad (16)$$
2 **5**

$$(\eta\text{-Cp})(CO)FeCOMe + PhSMe \xrightarrow{k_{17}} (\eta\text{-Cp})(CO)(PhSMe)FeCOMe \quad (17)$$
5 **4**

$$\text{rate} = k_{16}k_{17}[\mathbf{2}][PhSMe]/\{k_{-16}[Ac] + k_{17}[PhSMe]\} \quad (18)$$

$$[PhSMe]/k_{13} = [PhSMe]/k_{16} + k_{-16}[AC]/k_{17}k_{16} \quad (19)$$

should be linear as is shown in Figure 5. Analysis of these data using this model affords values for k_{16} (0.15 s^{-1}) and k_{-16}/k_{17} (6.8×10^{-3}). As expected, the transformation of $2^{0,+}$ to $4^{0,+}$ is thermodynamically more favored in the iron(II) state ($\Delta\Delta G° = -21.1$ kJ/mol; $K_0/K_+ = 3.7 \times 10^5$). This undoubtedly reflects the greater affinity of the soft acid iron(II) for the soft base PhSMe.

The acetone complex **2** decomposes slowly at −75 °C via a process that depends only on the concentration of the complex. Although we do not know the nature of the decomposition product, we reasonably speculate that it is the starting material $(\eta\text{-Cp})(CO)_2FeMe$ (**1**). The conversion of **2** to **1** is envisioned as occurring either via the slow rearrangement of the coordinatively unsaturated acetyl complex **5** or by rearrangement and simultaneous dissociation of acetone from **2**. The decomposition of **2** to **1** via intermediate **5** would exhibit a large positive entropy of activation. On the other hand, the concerted rearrangement of **2** to **1** would exhibit a small $\Delta S^‡$ which might be positive or negative depending on the nature of the transition state. The experimentally determined (Figure 5) value of -2.8 ± 7.8 eu for $\Delta S^‡$ appears to be more consistent with the concerted rearrangement than with the stepwise rearrangement of **2** to **1**.

A curious feature of this system is the apparently exclusive conversion of the iron(II) perchlorate complex 3^- to the sulfide complex **4**. At first glance, it would seem reasonable that both the acetone complex **2** and the perchlorate complex 3^- would dissociate to **5**. Clearly, this cannot be the case for 3^- since its decomposition via **5** would afford initially a 1:1 mixture of **2** and **4** (based on the value for $k_{-16}[AC]/k_{17}[PhSMe]$). Attempts to incorporate the decomposition of 3^- into equimolar amounts of **2** and **4** led an unsatisfactory fit of the simulations to the experimental data. This problem is currently under study.

Experimental Section

Electrochemistry. Electrochemical measurements were carried out on an EG&G PAR 174A polarographic analyzer or Model 273 potentiostat using a one-compartment cell with a three-electrode configuration. The cell was designed so that the SCE reference electrode (kept near 22 °C) was connected through a Luggin capillary to the cell which could be dipped in appropriate slush baths. A platinum disk was used as the working electrode. The electrolyte was 0.1 M lithium perchlorate or hexafluorophosphate. The concentrations of the solutions of $(\eta\text{-Cp})(CO)_2FeMe$ ranged between 2.5 and 25 mM as measured at room temperature. $(\eta\text{-Cp})(CO)_2FeMe$ was prepared by the metathesis between $(\eta\text{-Cp})(CO)_2Fe^-$ and dimethyl sulfate. The crude product was chromatographed on basic activity I alumina using petroleum ether as an eluent. The resulting material, which was crystallized at low temperatures, was vacuum sublimed prior to use. Reagent grade acetone was distilled from potassium carbonate prior to use. Slush baths of acetone, dimethylformamide, octane, acetonitrile, and dichloroethane were used to achieve appropriate temperatures that were measured at the beginning and end of each experiment. Thioanisole was vacuum distilled twice before use.

The experiments with thioanisole were complicated by appearance of a small amount of an electrochemically active material formed in the bulk and not at the electrode surface. We included this material in the simulations in order to get the appropriate shapes. The required concentration of this impurity was so small that it had virtually no effect on the values of the rate constants obtained from the simulations although its inclusion reproduced the curve shapes quite well.

Computer Simulations. The experiment being simulated is a combination potential step and linear sweep voltammetry. The system is described in Scheme I. The simulation is based on the method of finite differences.[8] In the step and hold part of the simulation, 1^+ is generated and converts into 2^+ and **3** which interconvert as shown in Scheme I. The concentration profiles of 2^+ and **3** at the end of the step and hold part of the experiment are computed in a subprogram. These are used as the initial conditions for the linear sweep portion of the simulation. The main program describes the linear sweep portion and computes the concentration profiles of all species as a function of time. After each time interval, the current is computed as proportional to the sum of concentration gradients of 2^+ and **3** at the solution/electrode interface. Uncompensated internal resistance and finite heterogeneous kinetics were treated collectively by employing the formalism of the Butler–Volmer equation. A common diffusion coefficient was used for all species. The various homogeneous and heterogeneous rate constants along with values of α and $E°$ were varied until the simulations fit the experimental curves from which the capacitive current had been subtracted. The set of equations was integrated by using the Adams–Bashforth[8] method of order 1. Owing to the sufficiently fine net employed, results differed insignificantly from those obtained by using the more accurate Adams–Moulton method in PECE form (second order in predictor, third order in corrector). This feature attests to the accuracy of the computer results. The code is provided in supplementary material. The homogeneous rate constants are given in Table I. The reduction potentials of the $2/2^+$ and $4/4^+$ couples were determined to be −0.016 and 0.203 V, respectively, versus an SCE electrode at 23 °C. We are unable to observe the return wave for the oxidation of 3^- after reduction of **3**. Therefore, the cathodic peak potential for the reduction of **3** is determined by a combination of the kinetics of the follow-up reaction of 3^- as well as the real $E°$ value for the $3^-/3$ couple. We chose an $E°$ value for the couple that reproduced the experimental data for the reduction of **3**. This $E°$ value must not be considered as the thermodynamic value for the $3^-/3$ couple.

Acknowledgment. We gratefully thank the donors of the Petroleum Research Fund, administered by the American Chemical Society, and the Graduate School of Boston University for support of this research.

Supplementary Material Available: The computer program for the simulation (3 pages). Ordering information is given on any current masthead page.

(8) (a) Shampine, L. F.; Gordon, M. K. *Computer Solution of Ordinary Differential Equations*; W. H. Freeman and Co.: San Francisco, 1975. (b) Vemuri, V.; Karplus, W. J. *Digital Computer Treatment of Partial Differential Equations*; Prentice-Hall: Englewood, Cliffs, NJ, 1981.